



Anti-inflammatory effects of FS48, the first potassium channel inhibitor from the salivary glands of the flea *Xenopsylla cheopis*

Received for publication, November 13, 2020, and in revised form, April 7, 2021 Published, Papers in Press, April 15, 2021,

<https://doi.org/10.1016/j.jbc.2021.100670>

Zhenhui Deng^{1,2,‡}, Qingye Zeng^{2,‡}, Jie Tang^{3,‡}, Bei Zhang², Jinwei Chai², John F. Andersen⁴ , Xin Chen^{1,*}, and Xueqing Xu^{2,*} 

From the ¹Department of Pulmonary and Critical Care Medicine, Zhujiang Hospital, ²Guangdong Provincial Key Laboratory of New Drug Screening, School of Pharmaceutical Sciences, and ³Department of Physiology, School of Basic Medical Sciences, Southern Medical University, Guangzhou, China; and ⁴Laboratory of Malaria and Vector Research, NIAID, National Institutes of Health, Bethesda, Maryland, USA

Edited by Mike Shipston

The voltage-gated potassium (Kv) 1.3 channel plays a crucial role in the immune responsiveness of T-lymphocytes and macrophages, presenting a potential target for treatment of immune- and inflammation related-diseases. FS48, a protein from the rodent flea *Xenopsylla cheopis*, shares the three disulfide bond feature of scorpion toxins. However, its three-dimensional structure and biological function are still unclear. In the present study, the structure of FS48 was evaluated by circular dichroism and homology modeling. We also described its *in vitro* ion channel activity using patch clamp recording and investigated its anti-inflammatory activity in LPS-induced Raw 264.7 macrophage cells and carrageenan-induced paw edema in mice. FS48 was found to adopt a common $\alpha\beta$ structure and contain an atypical dyad motif. It dose-dependently exhibited the Kv1.3 channel in Raw 264.7 and HEK 293T cells, and its ability to block the channel pore was demonstrated by the kinetics of activation and competition binding with tetraethylammonium. FS48 also downregulated the secretion of proinflammatory molecules NO, IL-1 β , TNF- α , and IL-6 by Raw 264.7 cells in a manner dependent on Kv1.3 channel blockage and the subsequent inactivation of the MAPK/NF- κ B pathways. Finally, we observed that FS48 inhibited the paw edema formation, tissue myeloperoxidase activity, and inflammatory cell infiltrations in carrageenan-treated mice. We therefore conclude that FS48 identified from the flea saliva is a novel potassium channel inhibitor displaying anti-inflammatory activity. This discovery will promote understanding of the bloodsucking mechanism of the flea and provide a new template molecule for the design of Kv1.3 channel blockers.

Voltage-gated potassium (Kv) channels play an important role in Ca²⁺ signaling, action potential repolarization, cellular proliferation, migration and secretion, and cell volume

regulation (1). Their crucial involvement in the above physiological processes makes Kv channels important targets in developing novel therapeutic drugs against cancer, autoimmune diseases, and some diseases related to neurological, metabolic, and cardiovascular disorders (1). As an example, Kv1.3 expressed on macrophages and effector memory T lymphocytes is a multifunctional Kv channel and the target of drugs modulating the immune system (2). As such, highly selective modulators and blockers of Kv1.3 are excellent drug development sources for autoimmune and inflammatory diseases.

Some venomous animals can capture prey and defend against predators by changing the excitability after activation or inhibition of Kv channels in excitable cells. It is therefore not surprising that these channels are targets of a variety of toxins from venomous animals (3) and many ion channel modulators have been identified from venomous animals such as scorpions, spiders, snakes, and so on. Over the course of long-term evolution, blood-feeding arthropods have gradually developed a rich array of pharmacological peptides and proteins, which are helpful to feed and overwhelm their host's defense system. Transcriptomic and proteomic data from different labs have suggested that defensive responses of host animals related to hemostasis, immunity, and inflammation can be modulated by these various kinds of components (4). However, only a few of the ion channel modulators or blockers are identified from the salivary glands of bloodsucking arthropods. For example, Vasotab can prolong the action potential and cause positive inotropism of isolated rat heart myocytes (5), Ra-KLP can activate maxiK channels in an *in vitro* system (6), and the active constituents in the salivary secretion of *Triatoma infestans* can suppress Na⁺ channels, decreasing the generation and conduction of nerve action potentials (5–7).

FS proteins identified in the salivary glands of the cat flea *Ctenocephalides felis* and the rat flea *Xenopsylla cheopis* (Rots) (8, 9) contain the conserved eight-cysteine structure and three-disulfide bridge motif feature of scorpion toxins (8). We previously reported that FS50 from the flea *X. cheopis* whose

[‡] These authors contributed equally to this work.

* For correspondence: Xueqing Xu, xu2003@smu.edu.cn; Xin Chen, chen_xin1020@163.com.

A new Kv1.3 inhibitor identified from *Xenopsylla cheopis*

sequence is similar to that of the FS-H antigen of *C. felis* is an inhibitor of the sodium channel $\text{Na}_v1.5$ and can elicit recovery from arrhythmia induced by BaCl_2 in rats and monkeys (10). Another FS protein from salivary glands of *X. cheopis*, FS48, shares extremely low sequence identity to FS50 and high identity to the FS-1 antigen of *C. felis*. Thus, FS48 is conceived to have different functions from FS50. In this study, we perform an in-depth investigation into the structure and function of FS48. We find that FS48 can effectively block Kv1.1, Kv1.2, and Kv1.3 channels in the same manner as classical scorpion K^+ channel toxins. As expected, FS48 displays anti-inflammatory effects *via* blocking Kv channels *in vivo*. Finally, a predicted structural model indicates that FS48 contains the common core $\alpha\beta$ structure while lacking the classic functional dyad motif of scorpion toxins. Thus, it seems that FS48 is a novel α -KTx toxin rather than a scorpion toxin mimic. The present work is the first detailed study of a Kv channel blocker from the salivary glands of a blood-feeding arthropod and will provide a view to understand the blood-sucking mechanism of the flea and serve as a novel drug template molecule useful for the design of new Kv1.3 blockers with high selectivity.

Results

Expression, purification, and characterization of FS48

To evaluate the function of FS48, we obtained the recombinant protein as described previously (10). As revealed by SDS-PAGE analysis, the FS48 fusion protein (23.38 kDa) was mainly expressed in the soluble fraction in BL21(λ DE3) (lane 5) (Fig. 1A, panel a). The His tag was separated from the recombinant peptide using enterokinase, and the 23.38 kDa fusion protein was successfully split into two products, the His tag in a 17 kDa fragment and remainder in a fragment of

6.324 kDa (lane 6). Two peaks from the uncleaved mixture were apparent when separated by cation exchange chromatography after HisTrap HP affinity column (Fig. 1A, panel b). The cleaved FS48 fusion protein was nearly pure after the repurification with a HisTrap HP affinity column with a large peak appearing after about 40 min (Fig. 1A, panel c). Finally, after application to a Superdex 75 column, the purified protein corresponding to FS48 was eluted at about 13 min, was collected manually, and lyophilized (Fig. 1A, panel d). Both MALDI-TOF-MS and SDS-PAGE analyses suggested that FS48 was expressed and purified successfully (Fig. 1, A and B). The concentration of endotoxin was less than 5 EU/kg, which is below the allowable endotoxin limits stipulated by the FDA for IV preparations and an acceptable concentration for cell-based experiments. A final FS48 yield of 1.8 mg/L was obtained, and the protein was stored at -20°C after freeze-drying.

Sequence alignment and structural analysis of FS48

FS48 had a peptide chain of 55 amino acids with 15 charged residues, which were widely distributed throughout the entire molecule (Fig. 2A). As its alignment with known scorpion toxins using Clustal W showed, FS48 shares less than 20% sequence homology but contains the three-disulfide bond feature of the well-characterized scorpion α -KTx toxins, which adopt a well-known cysteine-stabilized α/β scaffold. In addition, although the typical “functional dyad” presenting in Charybdotoxin (ChTX) did not exist in FS48 while residues C49-C55 were relatively conserved when compared with scorpion toxins such as Agitoxin-2 (AgTx-2) and ChTX (Fig. 2B). The circular dichroism (CD) spectra analysis showed that FS48 contained α -helix, β -sheet, and random coil in aqueous solution such as ChTX (Fig. 2C). The predicted

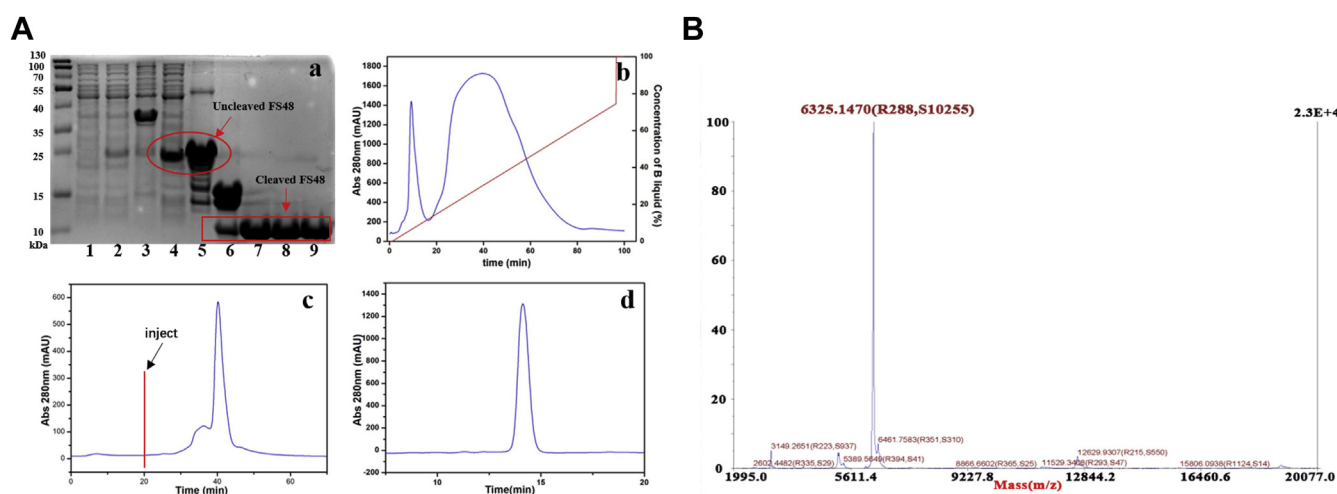


Figure 1. The expression, purification, and identification of FS48. A, SDS-PAGE analysis and chromatography purification of FS48. Panel a, SDS-PAGE images of expression and purification of FS48. Molecular mass markers (lane M); proteins from *E. coli* of BL₂₁ (λ DE₃) cells carrying pET-32a induced with IPTG for 12 h (lane 1); proteins from noninduced *E. coli* of BL₂₁ (λ DE₃) cells carrying pET-32a-FS48 (lane 2); insoluble proteins from *E. coli* of BL₂₁ (λ DE₃) cells carrying pET-32a-FS48 induced with IPTG for 12 h (lane 3); soluble proteins from *E. coli* of BL₂₁ (λ DE₃) cells carrying pET-32a-FS48 induced with IPTG for 12 h (lane 4); purified FS48 fusion protein after affinity chromatography and cation exchange chromatography (lane 5); fusion protein cleaved by enterokinase (lane 6); purified FS48 by the second affinity chromatography (lane 7); purified FS48 by gel filtration (lane 8); FS48 treated by Endotoxin Removal Kit (lane 9); panel b, Cation exchange chromatography column purification; panel c, HisTrap HP affinity column purification after enterokinase cleavage; panel d, Superdex⁷⁵ column purification. B, the purity and identity of FS48 was confirmed by MALDI-TOF-MS.

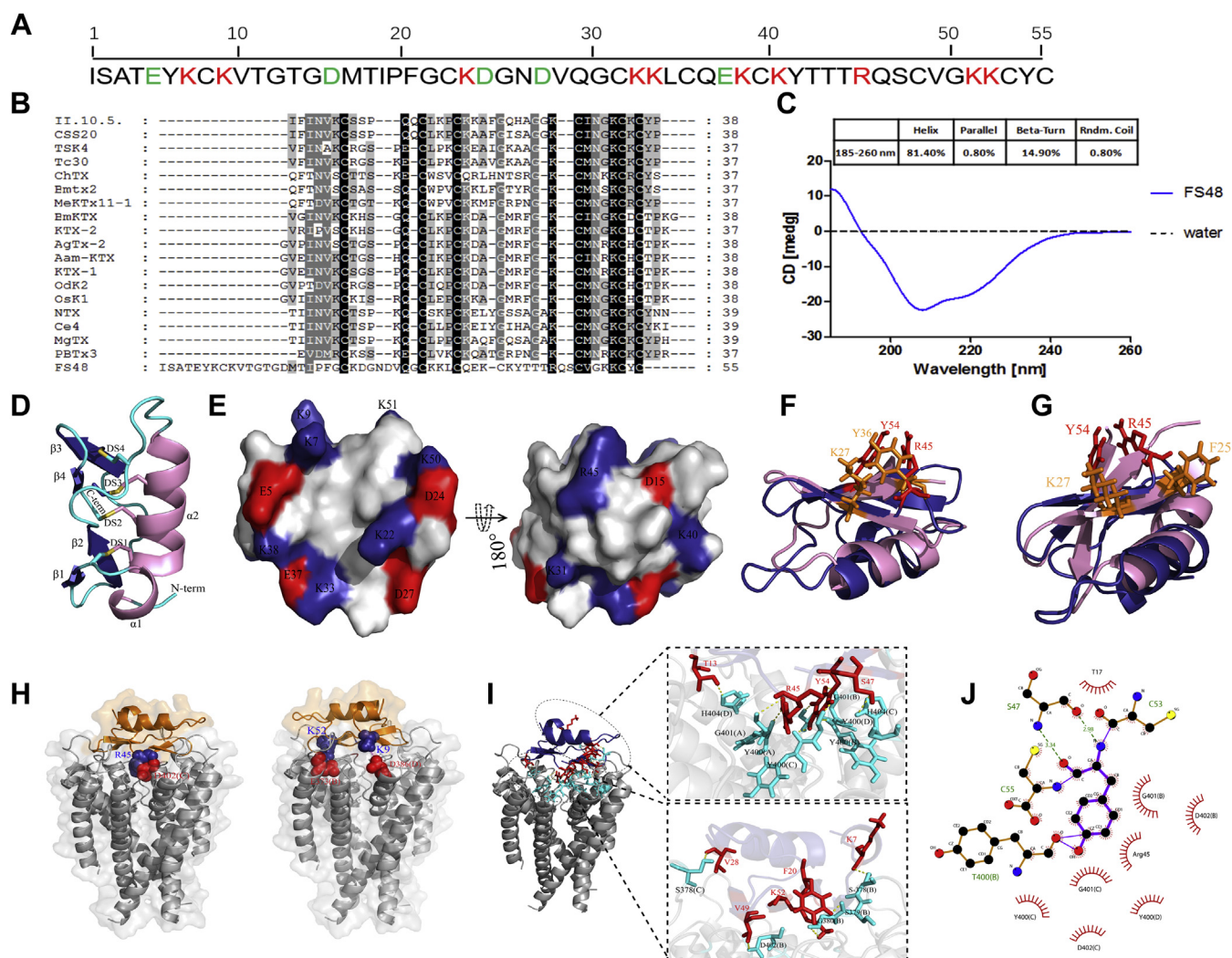


Figure 2. Sequence alignment and structural analysis of FS48. *A*, acidic and basic residue distributions of FS48 in its primary structure. *B*, sequence alignments of FS48 with well-known classic scorpion toxin peptides targeting Kv1.x channels. The *hyphens* (-) in some sequences denoted residue deletions to maximize structural similarity. The identical residues were indicated in black and the highly conserved residues were shadowed. UniProtKB Accession numbers were as followed: II.10.5 (C0HJW1), CSS20 (P85529), TSK4 (P46114), Tc30 (P60210), ChTX (P13487), Bmtx2 (Q9NII5), MeKTx11-1 (C0HJQ8), BmKTX (Q9NII7), KTX-2 (P45696), AgTx-2 (P46111), Aam-KTX (P0C8R1), KTX-1 (P24662), OdK2 (P0C909), OsK1 (P55896), NTX (P08815), Ce4 (P0C164), MgTX (P40755), PBTx3 (P83112.1). *C*, the CD spectra of FS48. Data were collected at 1-nm intervals with a continuous scan rate of 200 nm/min at 25 °C. *D*, Ribbon diagram of the FS48 monomer. The positions of α -helical (α 1- α 2) were in *light pink* and β -strand (β 1- β 4) structures in *deep blue*. Four disulfide bonds were displayed by yellow sticks and labeled by DS1-DS4 while the loops were marked in cyan. The N- and C-termini were also indicated. The homology model of FS48 was produced by ROSETTA server and visualized by Pymol. *E*, electrostatic potential surfaces of FS48. The surface was contoured with deep blue indicating positively charged areas while red indicating negatively charged region. Residues were labeled in shortened forms. Two views are related by a 180° rotation about the horizontal axis. *F* and *G*, structural superimposition of FS48 with Ctx and AgTx-2 with the putative dyad residues shown in stick models. *H*, the electrostatic interaction details of FS48-Kv1.3 complex. The complex was shown as surface model and the major function residues formed salt bridge within a contact distance of 6 Å were shown as sphere model and labeled. Basic residues K9, R45, and K52 of FS48 were colored in *deep blue*; acidic residues D386(D), D402(C), and E373(B) of Kv1.3 were colored in *red*. *I*, hydrogen bond interactions of FS48-Kv1.3 complex. *Panel*s in two boxes were the magnified images of the areas enclosed by two ellipses. The key functional residues at contacting regions were represented as stick model and colored in red and cyan for those from FS48 and Kv1.3, respectively. *J*, hydrophobic interactions of FS48-Kv1.3 complex around Y54 of FS48. The key residues involved in the hydrophobic interactions were labeled. The figure was prepared by LIGPLOT.

structure of FS48 was characterized by the presence of an α -helix with three turns running from V28 to C39 and a double-stranded antiparallel β -sheet composed of residues Q46-V49 and K52-C55. Two β -sheets were separated by a well-defined type I β -turn formed by the G50 plus K51 residues and connected by disulfide bridges, C31-C53 and C35-C55, to the α -helix and by disulfide C22-C48 to a loop spanning residues I18-D27, respectively. A tight turn formed by the residues K40-R45 separates the α -helix and the β -sheet. In addition, FS48 like FS50 contained an additional $\alpha\beta$ structure with a

small α -helix running from A3-Y6 and two strands of β -sheet spanning residues K9-T11 and G14-T17. Two structural regions were linked by the large loop spanning residues I18-D27 and the fourth disulfide bridge, C8-C39 (Fig. 2D). Of note, the surface of FS48 mainly consists of hydrophilic and polar amino acid residues, which are exposed to the solvent (Fig. 2E). Structural superimposition demonstrated that the overall fold of FS48 was very similar to those kv1.x channel blocking peptides such as AgTx-2 and ChTX (Fig. 2, F and G). Additionally, an atypical dyad comprising R45 and Y54 at the C

A new Kv1.3 inhibitor identified from *Xenopsylla cheopis*

terminus of FS48 could be well superimposed with that of ChTX at an ideal distance of about 6.8 Å between the carbon atom of R45 and the center of the aromatic ring of Y54 (Fig. 2, F and G).

Molecular mechanism of FS48 recognizing the Kv1.3 channel

To further explore the mechanism of FS48 blockade of the Kv1.3 channel, a reasonable FS48-Kv1.3 complex model was obtained through bioinformatics methods using Z-docking. As shown in Figure 2H, FS48 took its β -sheet domains as the major channel-interacting surface in contrast with the fact that almost all negatively charged residues excluding D15, such as E5, D25, D27 and E37, were situated in the nonbinding interface. Although FS48 did not contain conserved pore-blocking K27 and Y36 residues like most Kv1.x toxins (11), the equivalent R45 of FS48 may project its side chain into the selectivity filter of Kv1.3 channel and interact with the conserved pore-blocking domain GYGDM located in S5-S6 subunit of Kv1.3 through several hydrogen bonds and salt bridges (Fig. 2, H and I). The phenol ring of Y54 seems to make pivotal contacts between FS48 and the vestibule of Kv1.3 channel via additional four hydrogen bonds with Y400 and G401 locating different subunits (Fig. 2H). Moreover, Y54 might also interact with Kv1.3 through six hydrophobic interactions with GYD locating different subunits (Fig. 2J). K9

and 52K could react with D376 locating the D link and E374 locating the B link in the turret domain, thus playing the role of the additional positively charged residue of the toxin (Fig. 2H). In addition, several extra hydrogen bond interactions were localized in the binding interface. In detail, K7, F20, V49, and K52 of FS48 formed four hydrogen bonds with S378, S379, D402, and G380 locating the B link of S5-S6 subunit while V28 and S47 of FS48 formed two hydrogen bonds with S378 and H404 residues of the channel C chain and T13 of FS48 formed hydrogen bond with H404 residue of the channel D chain (Fig. 2I). Thus, the complex model suggested a structural model for FS48 binding to Kv1.3 channel.

Effect of FS48 on the potassium channels

Since primary structure sequence alignments showed that FS48 belonged to the cysteine-stabilized α/β fold, known as the scorpion toxin-like superfamily, and might have effects on Na⁺ and K⁺ channels (11), the effect of FS48 was first examined on DRG neurons and HEK 293T cells expressing human Kv1.1, Kv1.2, Kv1.3, Kv2.1, Kv4.1 with the whole-cell patch clamp technique. As displayed in Figure 3, under the administration of FS48, no change of inward currents was observed when TTX-S (Fig. 3A) and TTX-R Na⁺ channels (Fig. 3B) were activated by a -10 mV depolarization, indicating that both TTX-S and TTX-R Na⁺ channels on DRG neurons were FS48-

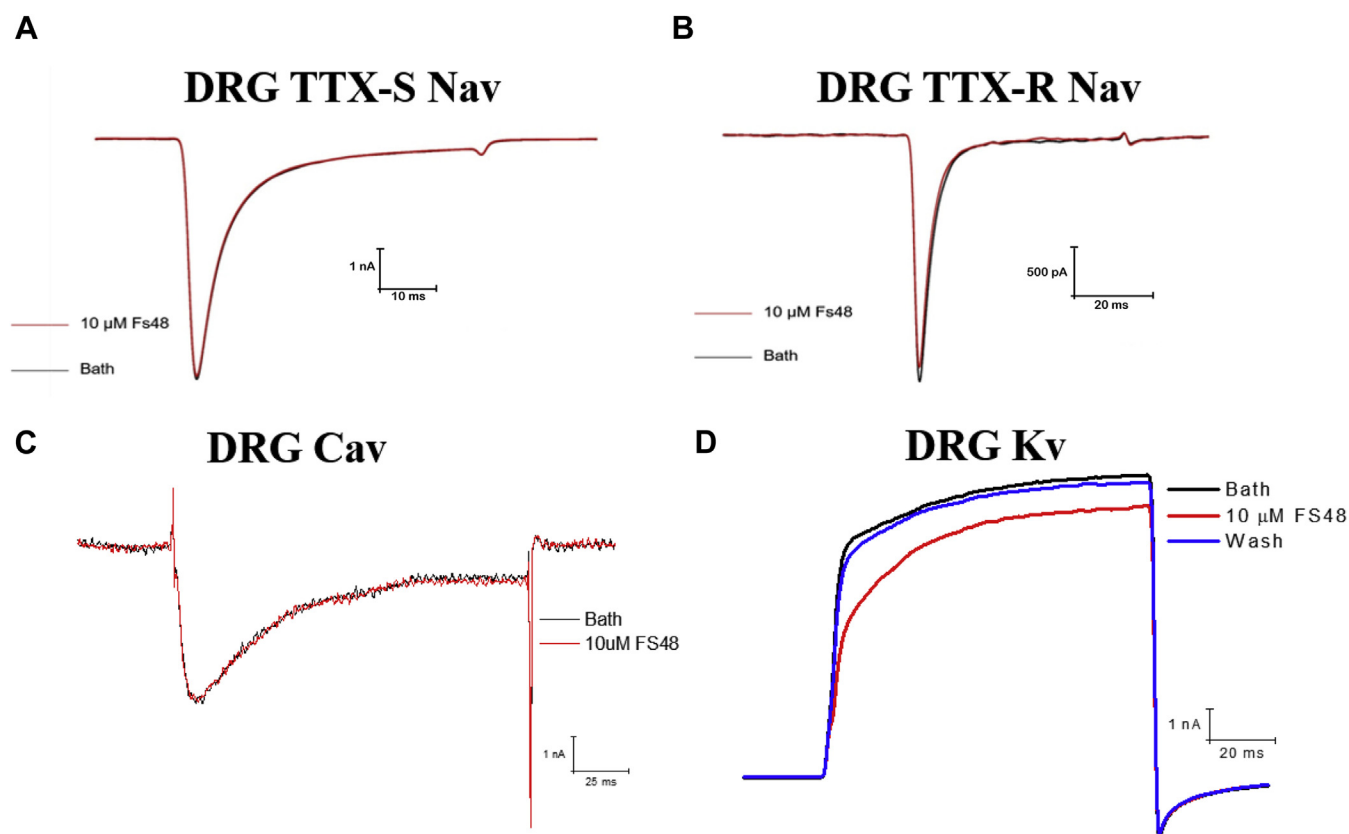


Figure 3. Effect of FS48 on Na⁺, Ca²⁺, and K⁺ channels on DRG. Na⁺ currents were elicited by a 50-ms depolarization to -10 mV from a holding potential of -80 mV. K⁺ and Ca²⁺ currents were elicited by a 100-ms depolarization to 0 mV from a holding potential of -80 mV. By comparing traces recorded before (black) and after (red) exposure to 10 μM FS48, no discernable change was found from TTX-S Na⁺ (A), TTX-R Na⁺ (B), and Ca²⁺ (C) rather than K⁺ (D). Scale bars are given as an inset.

resistant. The currents of Ca^{2+} channels on rat DRG cells were also completely insensitive to FS48 (Fig. 3C). For three neurons tested, 10 μM FS48 induced less than about a 3% decrease in current amplitudes of Na^{+} and Ca^{2+} channels. However, FS48 at 10 μM concentration reduced currents of K^{+} channels on rat DRG cells by about 12% (Fig. 3D, $n = 5$). The effects of FS48 on Kv channels were then determined on HEK 293T cells expressing Kv1.1–1.3, Kv2.1, and Kv4.1. The currents elicited by a +10 mV depolarization were measured before and after the application of FS48. As shown in Figure 4, FS48 at 10 μM had no effect on the currents in Kv2.1 and Kv4.1 expressing cells. However, the administration of 1 μM FS48 reduced by $42.77 \pm 3.09\%$, $23.52 \pm 1.08\%$, and $54.31 \pm 1.33\%$ the outward currents mediated by the Kv1.1–1.3 channels, respectively (Fig. 4, $n = 5$ for each group).

To further identify whether FS48 was an external pore blocker, a competition experiment with tetraethylammonium (TEA) was carried out. When 0.2 mM of TEA was added, the Kv1.1 current was reduced by $31.81 \pm 1.98\%$ ($n = 5$) (Fig. 4). However, when a mixture of 0.2 mM TEA and 1 μM FS48 was applied, the observed block was only increased by $7.5 \pm 1.3\%$ ($n = 5$), suggesting an obvious competition of both ligands binding Kv1.1 (Fig. 4). Thus, FS48, just as TEA, suppressed Kv1.1 by binding to the pore and occluding it.

The concentration-dependent effect of FS48 binding Kv1.1–1.3 was verified at concentrations ranging from 10 nM to 100 μM . Figure 5 shows the concentration-dependent suppression effects of FS48 on the currents of Kv1.1–1.3, producing IC_{50} values against the three subtypes of $1.34 \pm 0.12 \mu\text{M}$, $3.97 \pm 0.23 \mu\text{M}$, and $0.73 \pm 0.08 \mu\text{M}$, respectively (Fig. 5, A, E, and I). Notably, toward higher protein concentrations, the concentration–response curve showed saturation at above 95% inhibition of the K^{+} currents, suggesting that FS48 bound the channels with a high efficacy (Fig. 5, A, E, and I). Furthermore, the inhibition kinetics of FS48 were analyzed to identify the important role of the membrane depolarization

on its binding to three subtypes. 5 μM or 10 μM of FS48 caused a rapid suppression within about 12–16 s. However, the inhibition was readily reversible, and an almost complete recovery was observed after the washout with FS48-free external solution, with the time constant of 13 ± 3 s, which suggested an extracellular site of action (Fig. 5, B, F, and J).

The current–voltage relationships were explored with 200-ms voltage stimuli, ranging from -70 to $+20$ mV in a 10 mV step. As could be seen from the current–voltage curve before and after exposure to 1 μM FS48 (Fig. 5, C, G, and K), K^{+} currents were initially elicited at around -50 mV ($n = 5$). The maximum current was observed at $+20$ mV for the control. After treatment with 1 μM FS48, K^{+} current amplitudes at all test potentials were reduced. At 20 mV, the currents were decreased by $40.43 \pm 1.97\%$, $27.69 \pm 2.89\%$, and $47.5 \pm 2.34\%$, respectively (Fig. 5, C, G, and K). However, the voltage dependence of activation was not shifted by FS48, which implied that FS48 did not affect the voltage sensor of Kv1.1–1.3 subtypes. Additionally, the ratio of K^{+} current amplitude in the presence of peptide to one in its absence showed that the blocking effect of FS48 was voltage-independent. In order to elucidate whether FS48 inhibited the current through a physical obstruction of Kv channel pore or gating modification mechanism, the effects of FS48 on steady-state activation of Kv1.1–1.3 subtypes were investigated (Fig. 5, D, H, and L). The curves in the absence and presence of 1 μM FS48 were characterized by a $V_{1/2}$ values of -20.85 ± 0.69 mV and -22.62 ± 0.73 mV, -20.98 ± 0.14 mV and -21.22 ± 0.19 mV, -18.33 ± 0.13 mV and -18.83 ± 0.24 mV, respectively. Moreover, no significant changes were observed in the slopes of the curves before and after a 10-min exposure to 1 μM FS48. Thus, the cooperativity of the four voltage sensors of Kv1.1–1.3 subtypes was not affected by FS48 binding. Taken together, these results further indicated that FS48 performed its inhibitory effects *via* a voltage-independent pore-blocking mechanism.

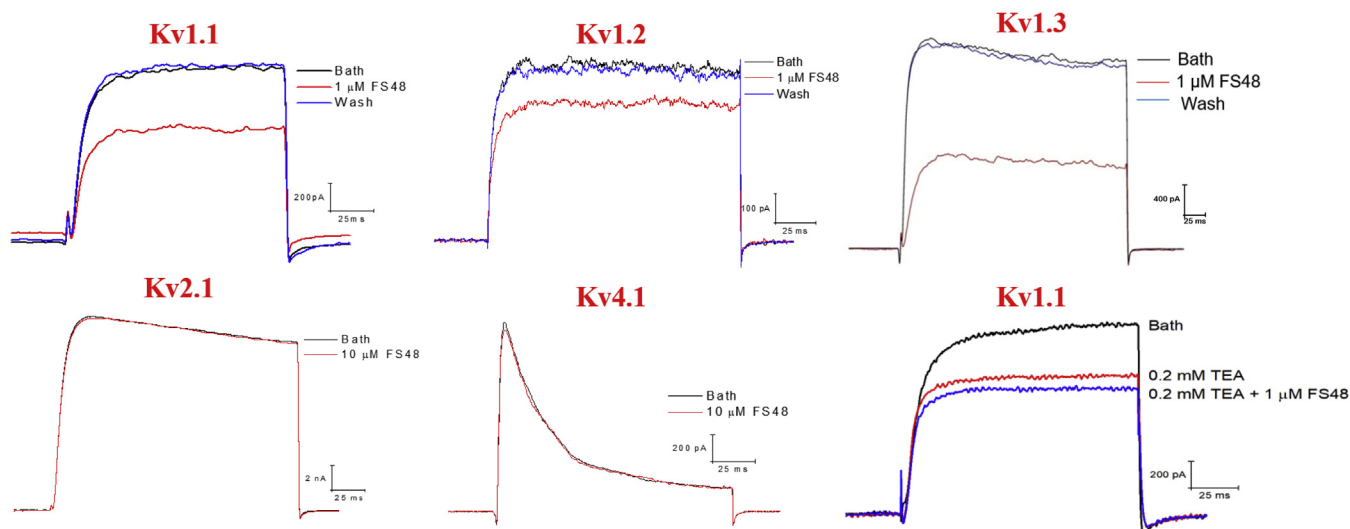


Figure 4. Pharmacological effects of FS48 on K^{+} channel subtypes. K^{+} currents were evoked by 100-ms depolarizing pulses to +10 mV from a holding potential of -70 mV. Representative currents traces of Kv4.1, Kv2.1, Kv1.1, Kv1.2, and Kv1.3 channels in the bath solution before (black line) and after (red line) the application of 1 μM or 10 μM FS48 and after (blue line) recovering by washout with the perfusion system. Scale bars are given as an inset.

A new Kv1.3 inhibitor identified from *Xenopsylla cheopis*

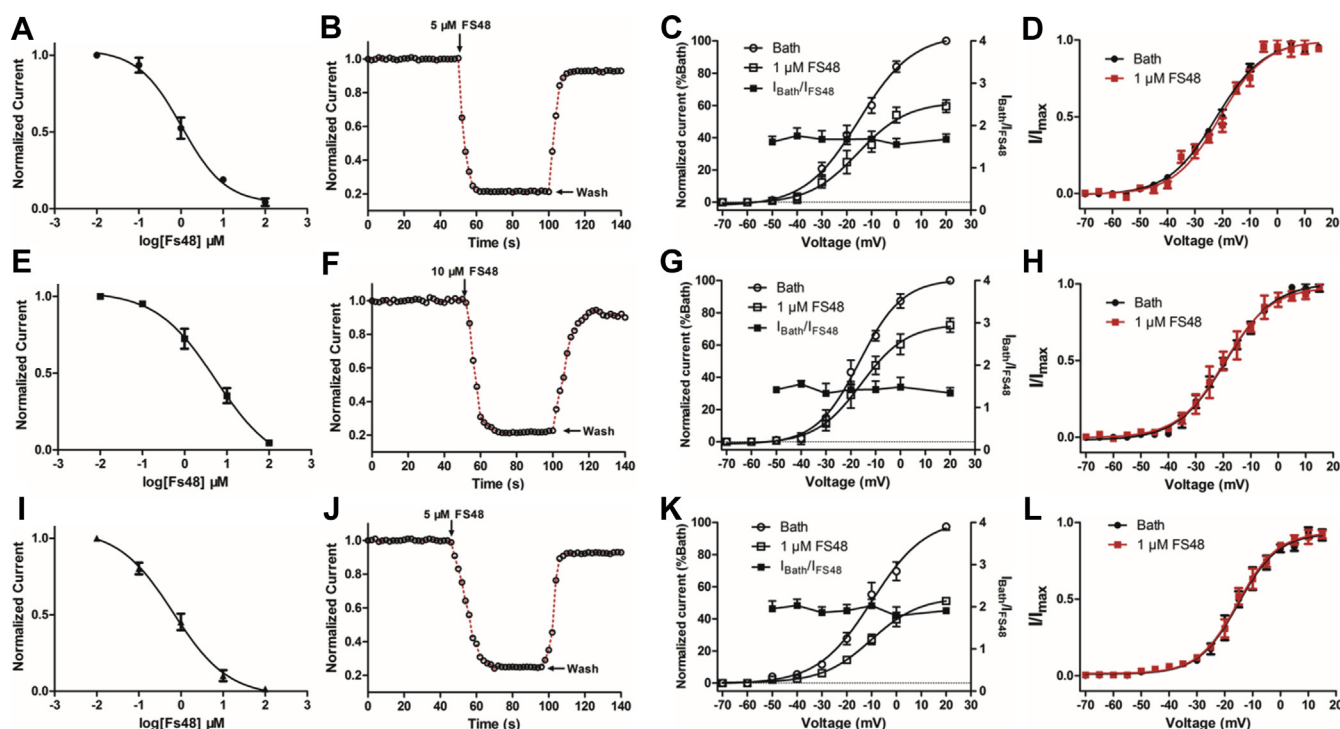


Figure 5. Functional features of FS48 blocking Kv1.1–1.3 channels. *A*, *E* and *I*, dose–response curves of FS48 inhibiting Kv1.1–1.3 were fitted with the Hill equation. Data represent mean \pm SEM of at least three experiments. *B*, *F*, and *J*, the time course of FS48 interacting with Kv1.1–1.3, respectively. Depolarizations were applied every 2 s by the voltage protocols. The addition and washout of 5 or 10 μ M FS48 in drug-free bathing solution were indicated by the bar. The representative elution plots were one of at least three individual experiments. *C*, *G*, and *K*, the current–voltage curves of Kv1.1–1.3 in the absence (*circles*) and the presence (*squares*) of 1 μ M FS48. Test potentials ranged from -70 mV to $+20$ mV at increments of $+10$ mV. Additionally, the voltage dependence of the block was shown by plotting the normalized currents at the end of the prepulse in the presence of 1 μ M FS48 as a function of the prepulse voltage (*filled squares*). *D*, *H*, and *L*, effects of FS48 on the activation of Kv1.1–1.3 channels. Activation curves were obtained by plotting the normalized tail currents of Kv1.1–1.3 as a function of the prepulse potential. The *solid lines* represent the average Boltzmann fits in the absence (*black dots*) and presence (*red squares*) of 1 μ M FS48. No significant curve shift was observed. Data represent mean \pm SEM of at least five experiments.

In order to identify the sites of interaction between FS48 and Kv1.3, we constructed two mutants with R45 to A and R45 to K and examined their effects on Kv1.3 currents after mutants were expressed and purified. The results showed that 200 nM FS48R45 K did not alter the activities suppressing Kv1.3 channel. However, 200 nM FS48R45 A markedly reduced its activities suppressing Kv1.3 channel when compared with 200 nM wild-type FS48 (Fig. S1).

Effects of FS48 on Kv currents of Raw 264.7 cells

Kv1.3 is highly expressed in activated macrophages and plays important roles in apoptosis, migration, phagocytosis, and immunomodulation of macrophages (12–15). To investigate whether FS48 had effects on the function of Kv channels of macrophages, the Kv currents evoked by depolarizing pulses in Raw 264.7 cells were measured under the administration of FS48. As shown by Figure 6A, at $+40$ mV, both 100 nM MgTx,

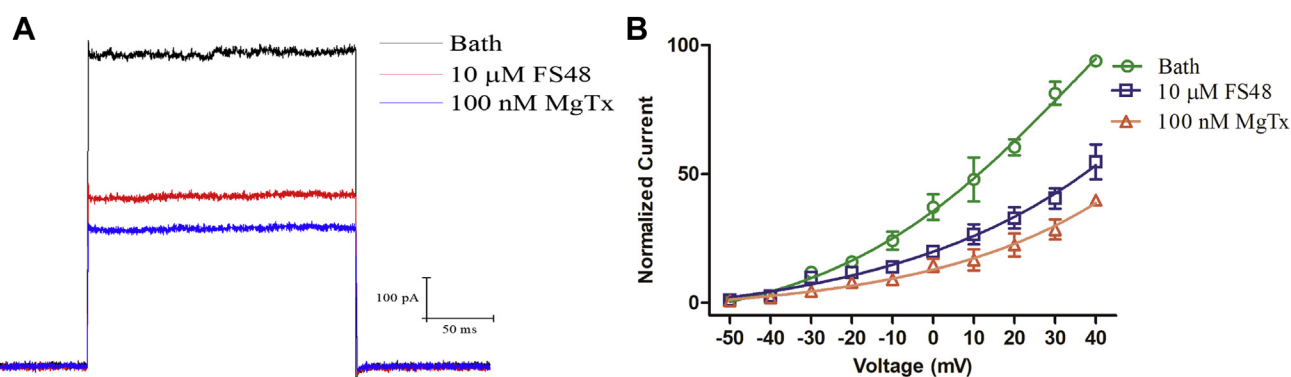


Figure 6. Effects of FS48 on Kv currents in Raw 264.7 macrophages. *A*, typical traces of K^+ currents in LPS-activated Raw 264.7 cells before (*black*) and after (*red*) perfusion with 10 μ M FS48 or (*blue*) 100 nM MgTx. Currents were elicited by applying 200 ms depolarization pulses from a holding potential of -70 mV to $+40$ mV. *B*, current–voltage relationships in the absence (*green circles*) or the presence of FS48 (*deepblue squares*) and MgTx (*tangerine triangles*) in LPS-activated Raw 264.7 cells. Test potentials were ranged from -50 mV to $+40$ mV at increments of $+10$ mV. Data represent mean \pm SEM of at least four experiments.

a highly specific Kv1.3 blocker, and 10 μM FS48 reduced the amplitude of the Kv current of LPS-activated macrophages by $59.45 \pm 2.79\%$ and $54.63 \pm 4.94\%$, respectively. The current-voltage relationships were analyzed by using 150-ms voltage steps, ranging from -50 to $+40$ mV in steps of 10 mV at 2 s intervals, as depicted in Figure 6B. Once the channels opened at around -50 mV, robust outward current increases were observed in LPS-activated Raw 264.7 cells at all depolarizing voltages applied from -50 to $+40$ mV (black line, $n = 4$). However, the currents at all test voltages were reduced markedly by the treatment with 1 μM FS48 (red line) or 100 nM MgTx (blue line).

Effect of FS48 on Kv1.3 channel mRNA and protein expression

Apart from acute inhibition of functional Kv1.3 channels, Kv1.3 blockers have been proven to exhibit anti-inflammatory and immunomodulatory effects by decreasing the channel expression (2). Before analysis, the cytotoxic effect of FS48 on murine macrophages was evaluated by the MTT method. As shown in Figure 7A, the addition of 0.1–30 μM FS48 to cells for 24 h did not inhibit the proliferation of Raw 264.7 cells. To analyze the effect of FS48 on Kv1.3 channel expression, Raw 264.7 cells activated by 100 ng/ml LPS were exposed to 3 μM FS48 and 100 nM MgTx for 24 h before the mRNA and protein expression of Kv1.3 were measured using real-time PCR and western blot analysis. FS48 and MgTx greatly reduced mRNA expression induced by LPS (Fig. 7B). Correspondingly, the amount of Kv1.3 protein elicited by LPS also was inhibited by FS48 and MgTx (Fig. 7C). On average, 3 μM FS48 and 100 nM MgTx decreased Kv1.3 protein expression induced by LPS by

$73.58 \pm 7.25\%$ and $76.15 \pm 13.81\%$, respectively (Fig. 7, C and D).

Inhibition of LPS-induced NO and inflammatory cytokines

As nitric oxide (NO) is an important indicator of macrophage activation, we explored the effects of FS48 on the NO production induced by LPS in Raw 264.7 cells. Compared with the control cells, Raw 264.7 cells stimulated by 100 ng/ml LPS showed a 59.78-fold increase of the mRNA level of iNOS. However, this increase was evidently inhibited by both MgTx and FS48 after exposure for 8 h (Fig. 8A). NO production is positively related to nitrite concentration in culture medium. Therefore, the NO secretion can be examined by determining the nitrite concentration in the supernatants of stimulated cells. As exhibited in Fig. 8B, 100 ng/ml LPS induced nitrite release increase from Raw 264.7 cells by 11.09 μM , but this increase was obviously inhibited by FS48 in a concentration-dependent manner after 24 h incubation. Furthermore, 10 μM FS48 had a similar effects to 100 nM MgTx with both inhibiting LPS-induced nitrite production by about 37.65%, which was in line with the results of mRNA levels.

To explore the effects of FS48 on LPS-stimulated inflammatory cytokines expression, the gene expression and protein production of TNF- α , IL-1 β , and IL-6 in Raw 264.7 macrophage cells were measured by quantitative real-time PCR (qRT-PCR) and ELISA with MgTx as the positive control. As shown in Figure 8, C–H, 100 ng/ml LPS significantly induced transcription and production of the above three inflammatory cytokines. Nevertheless, like MgTx, FS48 significantly blocked the production of TNF- α , IL-1 β , and IL-6 stimulated by LPS in a concentration-dependent manner.

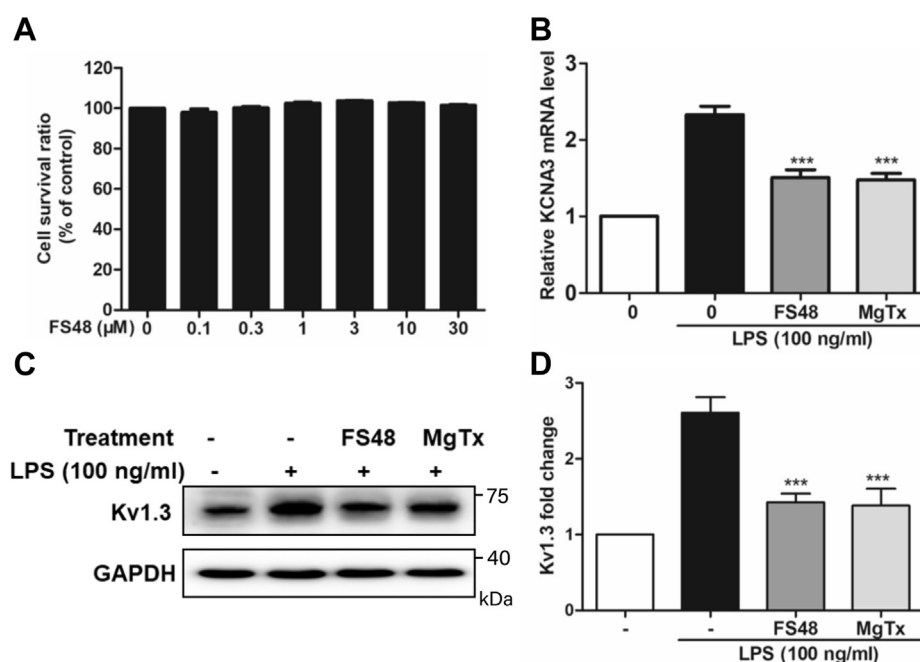


Figure 7. Effects of FS48 on the expression of Kv1.3 channel in Raw 264.7 macrophages. A, effects of FS48 on the viability of Raw 264.7 macrophages assessed by the MTT assay. B, the relative Kv1.3 mRNA contents in the absence and presence of FS48 and MgTx. C, representative western blot images of Kv1.3 protein expression in macrophages after 24 h incubation with FS48 and MgTx. D, quantitative analysis of Kv1.3 protein expression normalized to those of GAPDH shown in C. *** $p < 0.01$ versus control. Data represent mean \pm SEM of at least three experiments.

A new Kv1.3 inhibitor identified from *Xenopsylla cheopis*

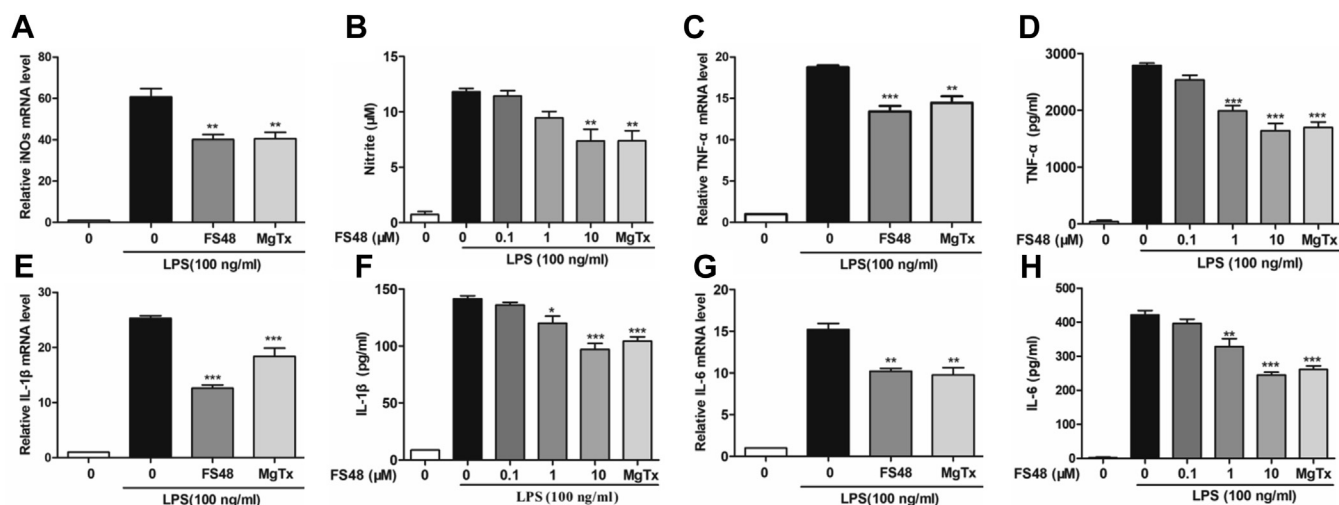


Figure 8. Effects of FS48 on NO and cytokine production induced by LPS. A, iNOS mRNA. B, NO production. C, TNF- α mRNA. D, TNF- α production. E, IL-1 β mRNA. F, IL-1 β production. G, IL-6 mRNA. H, IL-6 production. Expression of the target genes iNOS, TNF- α , IL-1 β , and IL-6 was measured by qRT-PCR and presented as fold change in the target genes expression normalized to GAPDH. Fold change of target genes expression in untreated cells was normalized to 1. NO, TNF- α , IL-1 β , and IL-6 in Raw 264.7 cell culture supernatant were determined by Griess reagent and ELISA, respectively. Data represent mean \pm SEM of at least three experiments. * $p < 0.05$, ** $p < 0.01$, and *** $p < 0.001$, compared with the control that was incubated with 100 ng/ml LPS.

Effects of FS48 on Raw 264.7 cells via Kv1.3

To identify whether the inhibitory effect of FS48 on macrophages was mediated by Kv1.3, Kv1.3 expression in Raw 264.7 cells was specifically knocked down using siRNA. Three siRNA sequences were employed, and western blot analysis revealed that the Kv1.3 level in all macrophages transfected with siRNA was obviously downregulated compared with nonsilencing RNA (Fig. 9A). Gene knockdown rates of Kv1.3 by Si-1, Si-2, and Si-3 in LPS-stimulated Raw 264.7 cells were

about $38 \pm 6.67\%$, $43.24 \pm 10.94\%$, and $91.4 \pm 1.84\%$, respectively (Fig. 9B). We then further studied the effects of FS48 on macrophages transfected with Si-3. As shown by Figure 9, C–F, the production of NO, TNF- α , IL-1 β , and IL-6 in Raw 264.7 cells stimulated by LPS was not affected by downregulation of the Kv1.3 channel and respectively showed 4.18, 26.13, 16.03, and 108.94-fold increases when compared with the control. However, the downregulation of the Kv1.3 channel greatly reduced the suppressive effects of both MgTx and

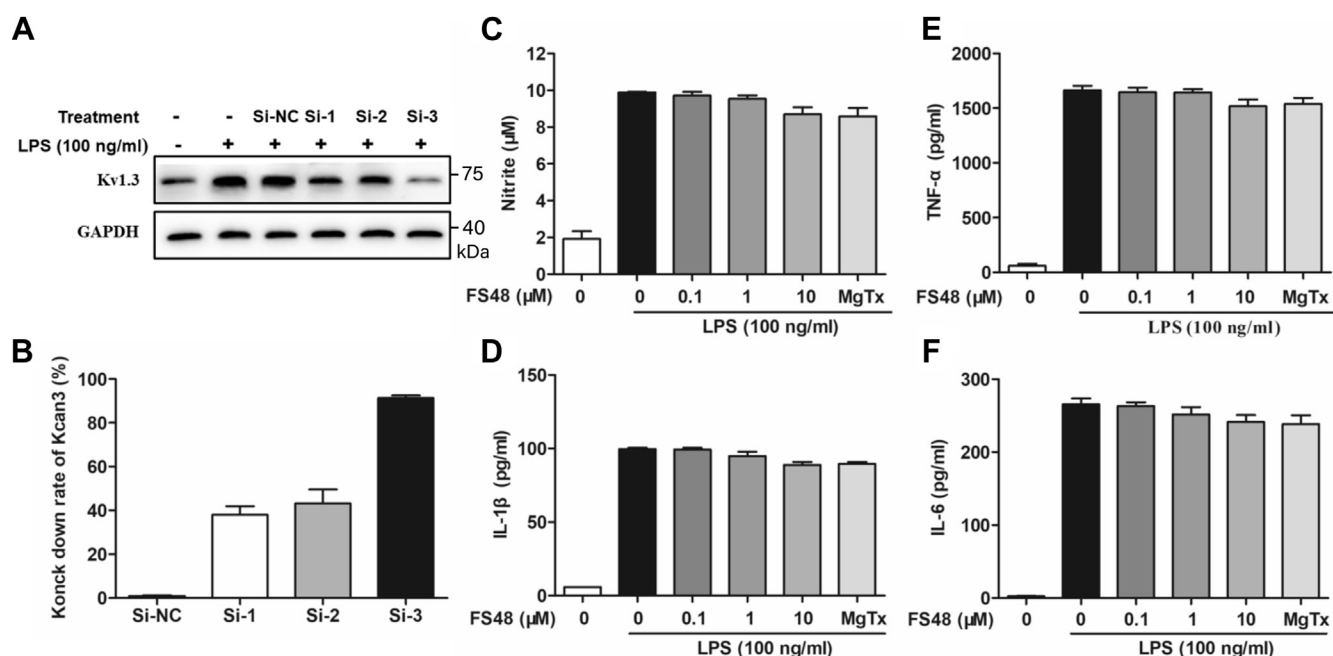


Figure 9. Effects of FS48 on NO and cytokine secretion in Raw 264.7 macrophages with Kv1.3 knockdowns. A, representative western blot images of Kv1.3 protein expression in macrophages knocked down by siRNAs. B, quantitative analysis of the Kv1.3 protein contents measured by western blot. C–F, effects of FS48 on NO and cytokine productions in LPS-stimulated Raw 264.7 macrophages with Kv1.3 knockdowns. The contents of NO, TNF- α , IL-1 β , and IL-6 in Raw 264.7 cell supernatant were measured by Griess reagent and ELISA kits, respectively. Data represent mean \pm SEM of at least four experiments.

FS48, which did not inhibit the production of NO, TNF- α , IL-1 β , and IL-6 in Raw 264.7 cells stimulated by LPS when compared with the control. The results confirmed that the blockage of Kv1.3 by FS48 was responsible for its suppressive effects on macrophage cells.

Inhibition of LPS-stimulated inflammatory response pathways

The Kv1.3 channel is closely associated with MAPK/NF- κ B pathways, which play key roles in the production of inflammatory cytokines (16, 17). Therefore, the effects of FS48 on LPS-stimulated inflammatory signaling pathways were investigated by western blot. As shown in Figure 10A, compared with normal cells, addition of 100 ng/ml LPS significantly activated MAPK/NF- κ B pathways and increased the amounts of phosphorylated ERK, JNK, p38, and the nuclear translocation of the NF- κ B p65 subunit. However, like the positive control, MgTx, FS48 evidently abrogated the increasing levels of phosphorylated ERK, JNK, p38, and nucleus translocation of NF- κ B p65 induced by LPS. Their reduction rates were 45.78 \pm 2.85%, 44.44 \pm 2.31%, 54.23 \pm 2.03%, and 44.25 \pm 7.04%, respectively (Fig. 10B). The results suggested that FS48 inhibited the inflammatory factor expression in LPS-activated macrophages *via* suppressing MAPK/NF- κ B signaling pathways.

Paw edema assay

The effect of FS48 in acute inflammation was identified with the carrageenan-induced paw edema assay with aspirin as the positive control. As illustrated in Figure 11A, the carrageenan administration triggered edema formation, which reached

peak at 4 h and then slowly declined but continued to exist until the end of the experiment at 24 h. Nevertheless, compared with a model group at 4 h, both aspirin and FS48 suppressed mouse hind paw edema induced by carrageenan approximately 44.79% and 37.02, respectively. Moreover, 24 h after injection, the edema induced by carrageenan was inhibited 49.32 \pm 7.78% and 53.05 \pm 22.34% ($p < 0.001$) when compared with a model group (Fig. 11B). In another set of experiments, carrageenan injection enhanced tissue myeloperoxidase (MPO) activity in the paws, which is a sign of the neutrophil assembling. However, the activities in the hind paw of aspirin and FS48-treated mice were reduced by 6.41 and 8.39 U/g tissue, respectively, compared with the carrageenan control group (Fig. 11C). The histological analysis of the intramuscular and epidermal structures of the carrageenan-injected hind paw is shown in Figure 11D. The inflammatory cells (small blue dots), which are a sign of inflammation, appeared in all paws stimulated with carrageenan. But, compared with the control group, the inflammatory cell infiltration was less intense and leukocyte infiltration was obviously reduced in the group treated with aspirin and FS48 (Fig. 11D). Especially, the group treated by aspirin showed nearly no inflammatory neutrophil cells. Thus, our results indicate that FS48 shows a significant anti-inflammatory effect, which is equal or slightly weaker than that of aspirin *in vivo*. The levels of proinflammatory cytokines in paw tissues stimulated by carrageenan were determined to further explore its anti-inflammatory mechanism *in vivo*. As illustrated in Figure 11E, carrageenan stimulation led to a significant increase in the secretion of IL-1 β , IL-6, and TNF- α in paw

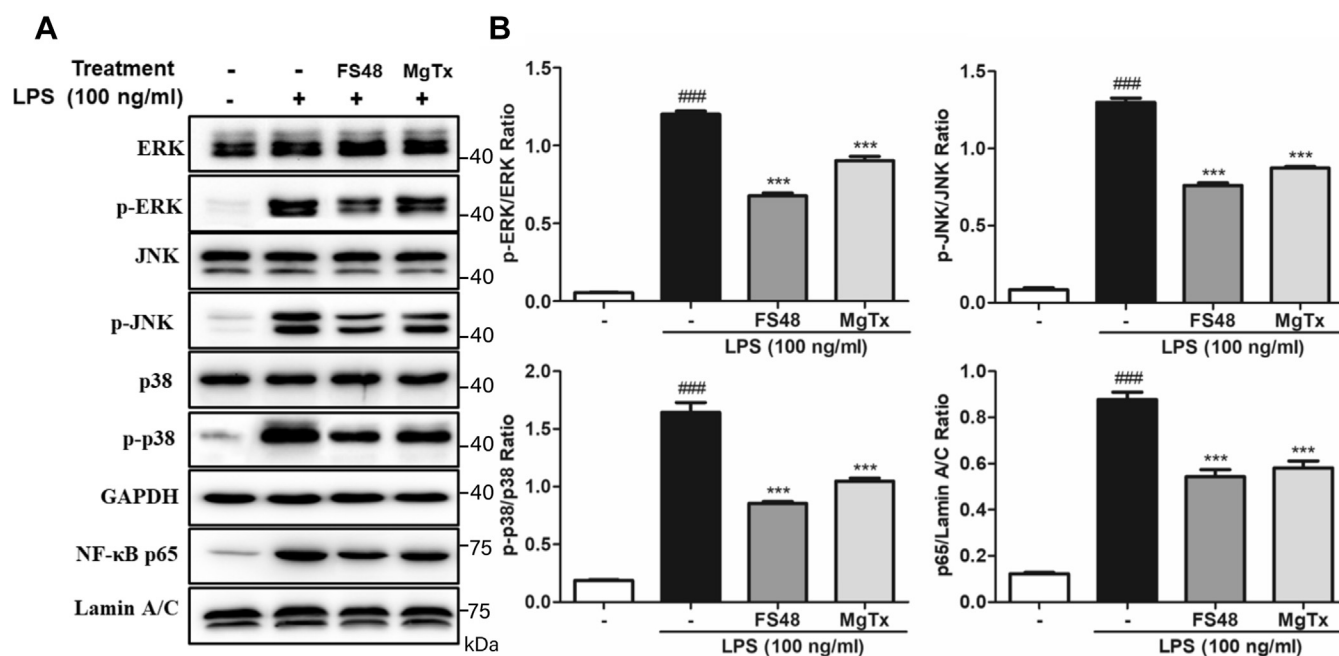


Figure 10. Effects of FS48 on LPS-activated inflammatory response pathways. A, representative western blot images of ERK, JNK, p38, and total p65 subunit in Raw 264.7 cells. The cells were treated with 100 ng/ml LPS and 3 μ M FS48 for 30 min with MgTx used as a positive control and then were collected for western blot analysis. B, ratio of phosphorylated ERK, JNK, p38 to corresponding total protein and p65 to Lamin A/C. Band densities were analyzed using Image J software (National Institutes of Health). Data represent mean \pm SEM of at least three experiments. *** $p < 0.001$, significance level compared with the control that was incubated with 100 ng/ml LPS. ### $p < 0.001$, significance level compared with the control without LPS and FS48.

A new Kv1.3 inhibitor identified from *Xenopsylla cheopis*

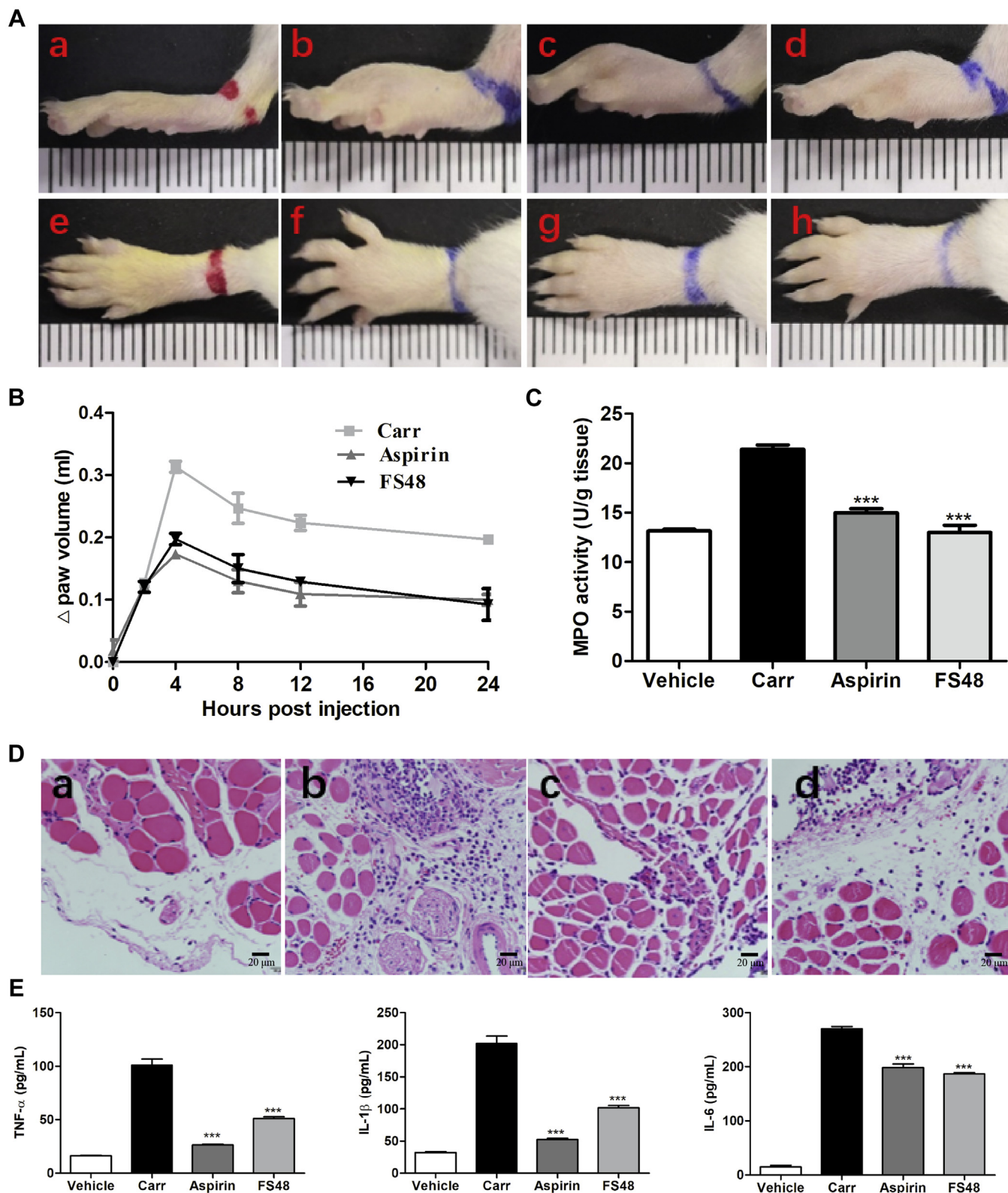


Figure 11. Anti-inflammatory effects of FS48 in mice. FS48 was administered intraperitoneally into mice 1 h before carrageenan (1%, 50 μ l) dissolved in saline was injected into the plantar side of right hind paw. Aspirin and saline solution were used as the positive and negative control, respectively. *A*, representative images of mouse paw edemas from saline (*a*, *e*), carrageenan plus saline (*b*, *f*), carrageenan plus FS48 (1.5 mg/kg) (*c*, *g*), carrageenan plus aspirin (5 mg/kg) (*d*, *h*) groups at 4 h post injection of carrageenan. The lateral and top views of paws are shown in *parts a–d* and *parts e–h*, respectively. The unit of scale bars shown in images *a–h* is the centimeter. *B*, the degree of swelling at each time point after carrageenan administration. *C*, MPO activity in the inflamed paws from saline, carrageenan plus saline, carrageenan plus FS48, carrageenan plus aspirin groups. *D*, histological analysis of mouse paws treated by saline alone (*a*), carrageenan plus saline (*b*), carrageenan plus aspirin (*c*), carrageenan plus FS48 (*d*) at 4 h after carrageenan administration. *E*, Proinflammatory cytokine expression in the inflamed foot pads. Statistical results are expressed as the mean \pm SEM ($n = 6$). *** $p < 0.001$, significantly different than the control treated with carrageenan alone.

tissues while compared with control group. Nevertheless, this effect was diminished after treatment with aspirin and FS48, which is completely consistent with its effects on inflammatory cell infiltration and paw volume measurement (Fig. 11E).

Discussion

A large number of peptide toxins that functionally block or suppress voltage-gated ion channels have been identified in the venoms of scorpions, snakes, spiders, bees, sea anemones, and marine cone snails (3). Although the interest on component identification in flea saliva started 12 years ago (8), it is unclear as to whether it contains Kv channel inhibitors. In the present study, FS48 from salivary glands of *X. cheopis* inhibits dose-dependently Kv1.1–1.3 channels through a pore-blocking mechanism. Furthermore, FS48 with both an $\alpha\beta\beta$ structure and atypical dyad motif also downregulates the production of proinflammatory factors by Raw 264.7 cells via Kv1.3 channel blockage and expression suppression as well as MAPK/NF- κ B pathway inactivation. Finally, FS48 inhibits the acute inflammatory response in mice.

It is well known that the three disulfide bond cysteine sequence called α/β motif is conserved in many functionally different pore blocker proteins including scorpion toxins (11, 18). Both FS48 and FS50 also possess the consensus C...CXXXC... C...CXC in their primary structures and the latter has been demonstrated to contain the features of scorpion toxins in its structure (10, 11, 19). In addition, it has been reported that a Q residue at the equivalent position R14 of MTX has the crucial role keeping a standard disulfide bond pattern like Pi4 (20) and FS48 has Q at the equivalent position (Fig. 2B). As a result, it is reasonable to assume that FS48 adopts the standard cysteine-stabilized α/β scaffold of scorpion toxins and contains a C₁–C₄, C₂–C₅, and C₃–C₆ disulphide bridge arrangement (11, 18). In agreement, it is confirmed by the structural model prediction (Fig. 2D). Notably, in spite of its identity to other known α -KTx scorpion toxins having the common disulfide bonding pattern, FS48 cannot be classified into any of the scorpion toxin groups due to a lack of similarity based on the Tytgat criterion (19), which establishes that toxins must be sorted based on their cysteine positions. Therefore, FS48 should be categorized to a new family of α -KTx K⁺ channel toxins. Interestingly, although FS48 shows low homology with reported Kv toxins and lacks a typical “functional dyad,” which has been usually considered as one usual characteristics of Kv1.x channel blocking toxins (Fig. 2) (11), electrophysiological experiments still indicate that FS48 is a Kv1.x blocker (Figs. 4 and 5). Thus, the amino acid sequence features of peptide toxins are not the exclusively critical determinants for their channel blocking activities (11). The lack of specific sequence features and the phylogenetic distance between fleas and scorpions also suggest that the two groups have independently evolved Kv channel blockers based on a similar structural motif.

The functional dyad to recognize K⁺ channels usually consists of a crucial K and a 6.6 ± 1.0 Å distant hydrophobic aromatic residue Y or F, which is located in different sites of

various toxins (19, 21). FS48 does not contain the dyad motif with a serine in place of K27 and lack of an aromatic residue following the last cysteine when compared with ChTX, a classic pore-blocking toxin from *Leiurus quinquestriatus hebraeus* (22) (Fig. 2). However, its residues located between the conserved C48 and C53 are similar to equivalent residues in the scorpion α -KTx subfamily. Additionally, Y54, two residues ahead of its equivalent position Y36 of ChTX, is nine positions downstream of positively charged R45, whose distance is also considered to be a general characteristic of the dyad motif of some high-selectivity K⁺ channel blockers from scorpion venoms (Fig. 2F). Furthermore, the classic dyad structure is unlikely to represent the sole molecular determinant of toxins involved in binding to ion channels (18) and some short-chain α -KTx toxins lacking such feature can also interact with different kinds of K⁺ channels. For example, the K[F/Y] motif is a common feature of some structurally dissimilar K⁺ channel-blocking peptides such as BGK, SHK, and HaTx2, which have similar function like K27 and Y36 in ChTX (18), yet scorpion toxins such as AgTx-2 from α -KTx's 3 only have an aromatic residue F at site 24 or 25 on the outside of the β -sheet, which is related to the reaction with the Kv1.x channels (11). Pi1, α -KTx's 11.x and 18.x (11, 18, 23, 24) likewise behave as a potent blocker of the Kv1.x channels despite the lack of the integrity of the dyad. Toxin peptides from snakes, scorpions, cone snails, and sea anemones interact with the negative charged outer crevice of Kv channels and mainly protrude the side chain of K in dyad structure into the channel pore upon blocking, covering the central pore like a cork in a bottle and occluding ion flow through the channel (1, 18, 24–26). Consistently, the R45 side chain of FS48 inserts into the channel pore and forms salt bridges with residues of the P-domain selectivity filter in our docking model (Fig. 2A). Additionally, as found in numerous toxins with dyad structure, aromatic Y54 in FS48 forms hydrogen bonds and hydrophobic interactions with conserved pore-blocking domain GYGD of Kv1.3 (Fig. 2, I and J). Thus, Y54 and R45 in FS48 may form the new type of functional dyad located on a channel binding face of the molecular surface. In line with it, the mutation R45 to A but not K significantly decreases the Kv1.3 suppression activity of FS48 (Fig. S1), which further reveals the critical role of cationic amino acids at the position of 45 in FS48. It is worth noting that cationic K9 and K52 like basic residues surrounding the pore-plugging K in Tc32, Pi1, and CoTX1 (23, 24, 26) play a key role through electrostatic interaction during the recognition, interaction, and correct positioning of FS48 on the Kv1.3 channel (Fig. 2, H and I) and FS48 should target an extraordinarily conservative domain of Kv1.1–1.3 channels, possibly the p-region located at the transmembrane segments between S5 and S6 because it blocks three Kv channels with nearly identical affinity values (Fig. 5A). Therefore, FS48 is a new Kv channel blocker via binding with the turret and filter domain.

Although both Kv1.3 and Kv1.5 are expressed in macrophages, Kv1.3 channels mainly contribute to Kv currents and are the main isoform responsible for controlling proliferation, migration, activation, and cytokine secretion of macrophages

A new Kv1.3 inhibitor identified from *Xenopsylla cheopis*

(12, 13, 15, 27). Therefore, functional changes of this channel will give rise to different intracellular signals and cellular responses in macrophages. On the basis of our finding that FS48 inhibits Kv1.3 (Figs. 4 and 5), we speculate that FS48 can also suppress electrophysiological properties and specific pharmacological response of macrophages by targeting their K⁺ channels. Unexpectedly, FS48, at concentrations lower than or equal to 30 μM, is not cytotoxic toward murine Raw 246.7 macrophages (Fig. 7A) although it inhibits the Kv currents in Raw 264.7 macrophages activated by LPS as expected (Fig. 6). It is reported that Kv1.3 expressed in the plasma membrane and the inner mitochondrial membrane have different functions (12, 15, 28). The membrane-permeant drugs such as PAP-1, Psora-4, and clofazimine very efficiently induce cell death of diverse cancer cells while the membrane-impermeant inhibitors such as ChTX and ShK even in high concentration cannot affect cell viability (29, 30), clearly indicating that the Kv1.3 located in plasma membrane itself is not responsible for the apoptotic response. Therefore, it is reasonable that FS48 as a membrane-impermeant inhibitor does not suppress the proliferation of Raw 264.7 cells. It is acknowledged that the functional activation state of macrophage cells has a great effect on their electrophysiological properties (15). Therefore, we used LPS as an activator for all experiments involving macrophages. LPS activates macrophages, leading to the secretion of bioactive molecules such as cytokines and the increase of Kv current as well as the Kv1.3 expressions in the complex (12, 31). In line with these observations, in our study, LPS increases the Kv1.3 expression and cytokine secretion. However, this increase is inhibited by FS48 at a concentration of 10 μM, which is selected according to the cytotoxic and preliminary patch clamp results (Fig. 8). Furthermore, the effects of FS48 on macrophages are abrogated by siRNA-mediated downregulation (Fig. 9). These results suggest that FS48 inhibits inflammation by blockade of Kv1.3, which is further confirmed by the fact that both FS48 and MgTx abolish Kv currents regardless of the immunomodulatory agent, LPS (12). Several studies have shown that the Kv1.3 channel mediates macrophage inflammation through the activation of MAPK/NF-κB signaling pathways (16, 17, 32). In this study, we find that MAPK/NF-κB pathways are activated in LPS-stimulated Raw 264.7 cells. Like MgTx, a commonly used antagonist in Kv.3 channel studies, FS48 prevents the activation of MAPK/NF-κB signaling pathways (Fig. 10), which is consistent with its inhibiting effects on Kv1.3 and cytokine expression, suggesting that FS48 can inhibit macrophage inflammation *via* suppression of Kv1.3 channel and consequently the MAPK/NF-κB signaling pathways.

Carrageenan-induced edema is generally used as an acute inflammation model and considered as a biphasic event: bradykinin, histamine, and 5-hydroxytryptamine are released in the first phase (0–1 h) (33). In contrast, various cytokines such as IL-1β, IL-6, and TNF-α are produced more actively in the second phase (after 1 h) (31, 32). It is reported that IL-1β and TNF-α can induce the recruitment of leukocytes such as neutrophils (34). In addition, polymorphonuclear cells, mobilized phagocytic cells, monocytes, and macrophages also

contribute to the second phase (35, 36). It is well acknowledged that Kv1.3 channels are expressed on immune cells including macrophages, dendritic cells, T-cells, and certain leukocytes (1, 2). Blockade of Kv1.3 channels on these cells also produces anti-inflammatory effects and immunomodulation (1, 2). For example, MgTx can suppress the maturation, migration, phagocytosis, inflammatory cytokines release, Kv-like currents, and Ca²⁺ influx of LPS-stimulated DCs (37). Consistently, MgTx is also reported to alleviate CCl₄-induced HF in mice through the regulation of cytokine secretion and the polarization of macrophages (38). Furthermore, according to another study by our group (unpublished data), FS48 has similar suppression effects of most Kv1.3 inhibitors reported on T cells and can relieve the delayed-type hypersensitivity response caused by skin-homing effector memory T cells. In present study, both FS48 and MgTx display remarkable anti-inflammatory effects on the second phase of carrageenan-induced paw edema (Figs. 11 and S2). In addition, FS48 can also inhibit inflammation and cytokines expression *via* inhibiting Kv1.3 channel and consequently the MAPK/NF-κB signaling pathways in macrophage. Thus, the anti-inflammatory effects of FS48 in carrageenan-induced mice maybe attributed to its suppression of immune cells including macrophages, neutrophils, dendritic cells, and T-cells, which express Kv1.3 channels on their cell membranes.

In conclusion, we have identified a Kv channel inhibitor from the flea saliva for the first time. FS48 with familiar αββ structure and atypical dyad motif exhibits a dose-dependently inhibitory activity against the channel Kv1.3 in Raw 264.7 cells and HEK 293T cells. Its pore-blocking mechanism is clear from the kinetics of activation and competition binding with tetraethylammonium. FS48 also downregulates the secretion of proinflammatory NO, IL-1β, IL-6, and TNF-α *via* Kv1.3 channel blockage and expression suppression as well as MAPK/NF-κB pathway inactivation in Raw 264.7 cells. Finally, FS48 inhibits the acute inflammatory response in mice. These discoveries will provide a view to understand the bloodsucking mechanism of flea and a novel drug template molecule with special structure for designing new Kv1.3 blockers.

Experimental procedures

Ethics statement

All experimental protocols involving animals were approved by the Animal Ethics Committee of Southern Medical University and were undertaken under the international regulations for animal research. Every effort was made to minimize the number of animals used and their sufferings.

Expression and purification of FS48

The cDNA sequence of FS48 (Genbank: ABM55450.1) was obtained according to our previous report (8) and the position of the signal sequence cleavage site was predicted using the program Signal-P (39). The cDNA sequence encoding mature FS48 followed by a stop codon was synthesized and cloned into the vector pET-32a *via* NcoI and XhoI restriction sites by GeneArt (Life Technologies). *E. coli* strain BL21 (ΔDE3) was

transformed with the expression plasmid and grown at 37 °C in LB with 100 mg/ml ampicillin. Cultures were cooled to 16 °C and fusion protein was induced by the addition of 0.8 mM isopropyl β -D-thiogalactoside (IPTG) at an OD₆₀₀ of 0.6. After 12 h cells were harvested by centrifugation, washed, and suspended with 20 mM Tris-HCl, pH 7.4, 0.2 mM phenylmethylsulfonyl fluoride, and finally broken by ultrasonication. The lysate was centrifuged at 30,000g and 10 °C for 30 min, and the supernatant was purified by HisTrap HP affinity column. The captured fusion protein was further purified by flowing through cation exchange chromatography on SP-sepharose before being cleaved by 0.2 mg/ml enterokinase (YEASEN Biotechnology) at 26 °C for 8 h. Recombinant FS48 was finally obtained by gel filtration purification with Superdex⁷⁵ column after the another additional HisTrap HP affinity column process for purification of the cleaved fusion protein. The residual endotoxin was efficiently detected and removed by ToxinSensor™ Chromogenic LAL Endotoxin Assay Kit and ToxinEraser Endotoxin Removal Kit (Genscript) according to the producer's manual. The identity of the recombinant FS48 was analyzed *via* MALDI-TOF MS with CHCA matrix on a 4700 Proteomics Bioanalyzer (Applied Biosystems) and by Edman degradation on an automated protein sequencer (Applied Biosystems).

Circular dichroism analysis

The secondary structure of FS48 in solvent environments was examined by CD spectroscopy using a Jasco-810 spectrophotometer (Jasco). The spectra at 180–260 nm were determined at 25 °C with 1 nm bandwidth, 1 s response time, and a scan speed of 100 nm/min in 0.1 cm path-length cell. Protein concentrations were approximately 100 μ M. Three consecutive scans were carried out and averaged, before subtraction of the buffer signal. All subtraction and processing were performed with the Jasco Standard Analysis Program. CD data were the mean residue ellipticity (θ) in deg·cm²·dmol⁻¹.

Structure computational modeling and docking

De novo molecular modeling of FS48 and the pore region of Kv1.3 channel was performed using the ROBETTA server and the SWISS-MODEL server with the structure of the KcsA channel (PDB code: 1BL8) as a template (40, 41). Using the modeled FS48 and Kv1.3 as templates, the FS48-Kv1.3 docking models were generated by ZDOCK program and the best Kv1.3-FS48 complex was chosen according to the Z Dock score combined with RMSD analysis as well as R-DOCK optimization (42). The solution structures of AgTx-2 and ChTX were retrieved from the Protein data bank (AgTx-2 PDB: 1AGT; ChTX PDB: 2CRD). The superimposition of FS48 with AgTx-2 and ChTX was performed by Align command in PyMOL software. Structure visualization was done with PyMOL without any refinement. Multiple sequence alignments of FS48 with previously characterized scorpion α -KTx toxins targeting Kv1.x channels were performed with ClustalW (<http://embnet.vital-it.ch/software/ClustalW.html>).

Animals and cell culture

Raw 264.7 macrophages and HEK 293T cells were from Shanghai cell bank of Chinese Academy of Science. The cells were cultured in Dulbecco's modified Eagle's medium, containing 10% FBS, 1% streptomycin/penicillin, and maintained at 37 °C under 5% CO₂. All animals were purchased from the Laboratory Animal Center of Southern Medical University and housed two per cage in a mini-barrier system of the central animal facility of Southern Medical University. Animals were bred with food and water freely in controlled environment with 60% humidity, 21 \pm 2 °C room temperature, and 12 h light–dark cycle.

Electrophysiological recordings

Rat DRG neurons were acutely separated and maintained in short-term primary culture, as previously described (10). Plasmids carrying human Kv channels (Kv1.1, Kv1.2, Kv1.3, Kv2.1, Kv4.1) and enhanced green fluorescent protein were from the Laboratory of Animal Models and Human Disease Mechanisms, Kunming Institute of Zoology, Chinese Academy of Sciences. Transient cotransfection of plasmids into HEK 293T cells were carried out with Lipofectamine 3000 (Invitrogen) according to the manufacturer's instructions for 24–48 h before electrophysiology analysis. Recording pipettes were fabricated from borosilicate glass capillaries using a P-97 horizontal micropipette puller (Sutter Instrument Company) and heat polished. Whole-cell patch clamp recordings were performed at room temperature using a MultiClamp 700B amplifier interfaced to a Digidata 1440A data acquisition system (Molecular Devices) unless otherwise stated. The data were filtered at 2 kHz and digitized at 20 kHz. Series resistance typically ranged from 6.0 to 8.0 m Ω and was compensated to 80% to minimize voltage errors. Unless otherwise stated, all reagents were obtained from Sigma. The components of the internal pipette and external bathing solutions at pH 7.2 for different ionic channel currents analysis are listed in Table S1. FS48 was dissolved in the external solution for the electrophysiological experiments and was applied with a fast perfusion system (A multichannel microperfusion system RSC-200, Bio-Logic USA). The liquid junction potential for these solutions was less than 8 mV and the resting potential was held at -70 mV for 4 min to allow adequate equilibration between the cell interior and the micropipette solution after establishing the whole-cell recording configuration. The offset potential was zeroed before contacting the cell. Kv currents were elicited by 200 ms depolarizing pulses to +20 mV from a holding potential of -70 mV every 2 s. Data were fitted with the Hill equation: $Y = 100 / (1 + 10^{-((\text{Log}IC_{50} - X) \times H)})$ (where y is the a normalized response, X is the log of concentration, and H is the slope factor or Hill slope) to identify the concentration–response relationships. To explore the current–voltage relationship and the voltage dependence of activation, Kv1.1–1.3 channel currents were evoked by the step pulses ranging from -120 to +40 mV for 200 ms with the increments of 10 mV while held at -120 mV at the beginning. The data points were fitted to the Boltzmann equation: $I/I_{\text{max}} = 1 / [1 +$

A new Kv1.3 inhibitor identified from *Xenopsylla cheopis*

exp $(V - V_{1/2})/k$ where k is the slope factor and $V_{1/2}$ is the voltage for half-maximum activation.

Cell viability assay

Cell viability of FS48 on Raw 264.7 macrophages was detected by the MTT assay as described previously (43). In brief, 5×10^3 /well Raw 264.7 macrophage cells were seeded into 96-well plates and allowed to grow overnight. Then the cells were treated with FS48 at the concentrations of 0.1–30 μ M for 24 h. After 10 μ l of MTT reagent (Sigma Aldrich) with a final concentration of 0.5 mg/ml was added to each well and incubated at 37 °C for 4 h, the formazan crystals were dissolved by addition of 200 μ l of dimethyl sulfoxide and absorbance was read at 570 nm using a microplate reader from Tecan Company. All experiments were conducted in four repeats. Cell viability was presented as a percentage of the nonstimulated control group.

Inflammatory cytokine measurement

5×10^4 cells/well of Raw 264.7 macrophages were plated in a 96-well culture plate and allowed to grow overnight. The cells were then coincubated with FS48 at the concentrations of 0.1–10 μ M and 100 ng/ml LPS (*E. coli* O₅₅:B₅, L6529, Sigma-Aldrich) for 24 h. After centrifugation, the culture supernatants were used to determine nitrite, TNF- α , IL-1 β , and IL-6 contents with Griess reagent (Sigma-Aldrich) and ELISA kits (eBiosciences) according to the manufacturer's instructions, respectively. The absorbance was read at 540 or 450 nm with a microplate reader (TECAN Company). The cells were treated with 100 nM MgTx as the positive control while cells without FS48 and/or LPS were used as the negative control. All experiments were repeated four times.

Quantitative real-time PCR

The total RNA was extracted with the Trizol reagent and quantified with a Merinton SMA100 (Merinton) after Raw 264.7 macrophage cells (2×10^5 cells/well) were treated by 3 μ M FS48 plus 100 ng/ml LPS for 8 h. qRT-PCR was performed with an ABI prism 7500 sequence detection system (Applied Biosystems) and SYBR premix Ex Taq (Tli RNaseH plus, Takara Company). The primer sequences for qRT-PCR are listed in Table S2 as previously described by us (44). The reaction cycles for all genes were performed under the following conditions: 95 °C for 5 min; 40 cycles at 95 °C for 15 s and 60 °C for 45 s. The threshold cycle was defined as the fractional cycle number at which the fluorescence passed the fixed threshold. The GAPDH gene was used as the control and internal standard to verify equal initial quantities of RNA. The expression of the target genes was normalized to the GAPDH gene and all experiments were carried out in triplicate.

siRNA transfection

The sequences of siRNA against Kv1.3 were Si-1 (sense: 5'-GCUUCUGGUGCGGUUCUUTT-3', antisense: 5'-AAA GAACCGCACCAGGAAGCTT-3'), Si-2 (sense: 5'-CCACU UGCACCACGAACAATT-3', antisense: 5'-UUGUUCGUG

GUGCAAGUGGTT-3'), Si-3: (sense: 5'-GCAGUAGUAA CCAUGACAATT-3', antisense: 5'-UUGUCAUGGUUACC ACUGCTT-3'); the sequences of nonsilencing RNA were Si-NC (sense: 5'-UUCUCCGAACGUGUCACGUTT-3', antisense: 5'-ACGUGACACGUUCGGAGAATT-3'). siRNAs were transfected into the Raw 264.7 cells at 1×10^5 cells/dish with Lipofectamine 2000 according to the manufacturer's manual. Western blot analysis was performed to evaluate the knockdown rate of the Kv1.3 channel protein.

Western blot analysis

1×10^6 Raw 264.7 macrophage cells were seeded into six-well plates. After respective incubation with 3 μ M FS48 and 100 nM MgTx, the cells were stimulated with LPS (0, 100 ng/ml) for 30 min and then collected for the extraction of the nuclear or cytoplasmic proteins. Western blot analysis was performed with primary antibodies against phospho-ERK/ERK, phospho-JNK/JNK, phospho-p38/p38, NF- κ B p65, Kv1.3, GAPDH and Lamin A/C (1:2000, 4 °C, overnight; Cell Signaling Technology), and horseradish-peroxidase-conjugated secondary antibodies (1:2000, 25 °C, 1 h) as described in our previous method (45). The bound antibody was detected with Immobilon Western chemiluminescent HRP substrate (Millipore) and Kodak XAR film. The band densities were quantified by Image J software and all experiments were performed in triplicates.

Paw edema assay

The carrageenan-induced paw edema model was performed to evaluate the anti-inflammatory activity as described in our previous study (44). Briefly, both male and female Kunming mice were at random divided into four groups with six animals each and their paw volume up to the ankle joint was determined with plethysmometer (Taimeng PV-200 7500). Subsequently, FS48 (1.5 mg/kg), saline, or aspirin (5 mg/kg) was administered intraperitoneally into mice 1 h before carrageenan (1%, 50 μ l) dissolved in saline was injected into the plantar side of right hind paw. The paw volume was then determined at 2, 4, 8, 12, and 24 h time point after carrageenan administration. The degree of swelling was expressed as the Δ volume (a-b), where "a" was the volume of right hind paw after carrageenan injection and "b" was the volume before the injection. In the secondary experiment, another set of mice were injected consecutively with FS48, aspirin, saline, and carrageenan as reported above. The right hind paws of all mice were surgically separated at 4 h after carrageenan injection for the histological analysis, cytokine measurement, and MPO activity assay.

Data analysis

qRT-PCR data were analyzed using the $2^{-\Delta\Delta CT}$ method (46). Statistical analysis was carried out using GraphPad Prism 5 software (GraphPad Software Inc). One-way analysis of variance with a post-hoc Dunnett test was used to investigate significance when comparing two or more groups with a control group and with a post-hoc Tukey test when

performing comparisons among three or more groups. The unpaired Student's *t*-test or one-way ANOVA was used to determine significance between two experimental groups. **p* < 0.05, ***p* < 0.01, and ****p* < 0.001 were considered statistically significant as compared with control.

Data availability

All data presented and discussed are contained within the article.

Supporting information—This article contains supporting information (44).

Acknowledgments—This study was funded in part by the National Natural Science Foundation of China (No. 31370782, 31861143050, 82070038, 31772476, and 31911530077).

Author contributions—Z. D., Q. Z., J. T., B. Z., and J. C. performed the experiments and analyzed data; J. F. A. designed the experiments and revised the article for publication; X. C. participated in study design and coordination and analyzed the data. X. X. designed and performed the experiments, supervised the study, evaluated the data, and revised the article for publication. All the authors contributed to the article and have given approval to the final version of the article. The article was written through contributions of all the authors.

Conflict of interest—The authors declare that they have no conflicts of interest with the contents of this article.

Abbreviations—The abbreviations used are: AgTx-2, Agitoxin-2; CD, circular dichroism; ChTX, Charybdotoxin.

References

- Wulff, H., Castle, N. A., and Pardo, L. A. (2009) Voltage-gated potassium channels as therapeutic targets. *Nat. Rev. Drug Discov.* **8**, 982–1001
- Serrano-Albarras, A., Estadella, I., Cirera-Rocosa, S., Navarro-Perez, M., and Felipe, A. (2018) Kv1.3: A multifunctional channel with many pathological implications. *Expert Opin. Ther. Targets* **22**, 101–105
- Norton, R. S., and Chandy, K. G. (2017) Venom-derived peptide inhibitors of voltage-gated potassium channels. *Neuropharmacology* **127**, 124–138
- Mans, B. J. (2011) Evolution of vertebrate hemostatic and inflammatory control mechanisms in blood-feeding arthropods. *J. Innate Immun.* **3**, 41–51
- Takac, P., Nunn, M. A., Meszaros, J., Pechanova, O., Vrbjar, N., Vlasakova, P., Kozanek, M., Kazimirova, M., Hart, G., Nuttall, P. A., and Labuda, M. (2006) Vasotab, a vasoactive peptide from horse fly *Hybomitra bimaculata* (Diptera, Tabanidae) salivary glands. *J. Exp. Biol.* **209**, 343–352
- Paesen, G. C., Siebold, C., Dallas, M. L., Peers, C., Harlos, K., Nuttall, P. A., Nunn, M. A., Stuart, D. I., and Esnouf, R. M. (2009) An ion-channel modulator from the saliva of the brown ear tick has a highly modified Kunitz/BPTI structure. *J. Mol. Biol.* **389**, 734–747
- Dan, A., Pereira, M. H., Pesquero, J. L., Diotaiuti, L., and Beirao, P. S. (1999) Action of the saliva of *Triatoma infestans* (Heteroptera: Reduviidae) on sodium channels. *J. Med. Entomol.* **36**, 875–879
- Andersen, J. F., Hinnebusch, B. J., Lucas, D. A., Conrads, T. P., Veenstra, T. D., Pham, V. M., and Ribeiro, J. M. (2007) An insight into the salivome of the oriental rat flea, *Xenopsylla cheopis* (rosts). *BMC Genomics* **8**, 102
- Ribeiro, J. M., Assumpcao, T. C., Ma, D., Alvarenga, P. H., Pham, V. M., Andersen, J. F., Francischetti, I. M., and Macaluso, K. R. (2012) An insight into the saliotranscriptome of the cat flea, *Ctenocephalides felis*. *PLoS One* **7**, e44612
- Xu, X., Zhang, B., Yang, S., An, S., Ribeiro, J. M., and Andersen, J. F. (2016) Structure and function of FS50, a salivary protein from the flea *Xenopsylla cheopis* that blocks the sodium channel NaV1.5. *Sci. Rep.* **6**, 36574
- Rodriguez, D. L. V. R., and Possani, L. D. (2004) Current views on scorpion toxins specific for K⁺-channels. *Toxicon* **43**, 865–875
- Villalonga, N., David, M., Bielanska, J., Vicente, R., Comes, N., Valenzuela, C., and Felipe, A. (2010) Immunomodulation of voltage-dependent K⁺ channels in macrophages: Molecular and biophysical consequences. *J. Gen. Physiol.* **135**, 135–147
- Leanza, L., Zoratti, M., Gulbins, E., and Szabo, I. (2012) Induction of apoptosis in macrophages via Kv1.3 and Kv1.5 potassium channels. *Curr. Med. Chem.* **19**, 5394–5404
- Zhu, H., Yan, L., Gu, J., Hao, W., and Cao, J. (2015) Kv1.3 channel blockade enhances the phagocytic function of RAW264.7 macrophages. *Sci. China Life Sci.* **58**, 867–875
- Vicente, R., Escalada, A., Coma, M., Fuster, G., Sanchez-Tillo, E., Lopez-Iglesias, C., Soler, C., Solsona, C., Celada, A., and Felipe, A. (2003) Differential voltage-dependent K⁺ channel responses during proliferation and activation in macrophages. *J. Biol. Chem.* **278**, 46307–46320
- Kan, X. H., Gao, H. Q., Ma, Z. Y., Liu, L., Ling, M. Y., and Wang, Y. Y. (2016) Kv1.3 potassium channel mediates macrophage migration in atherosclerosis by regulating ERK activity. *Arch. Biochem. Biophys.* **591**, 150–156
- Zhou, Q. L., Wang, T. Y., Li, M., and Shang, Y. X. (2018) Alleviating airway inflammation by inhibiting ERK-NF- κ B signaling pathway by blocking Kv1.3 channels. *Int. Immunopharmacol.* **63**, 110–118
- Mouhat, S., Jouirou, B., Mosbah, A., De Waard, M., and Sabatier, J. M. (2004) Diversity of folds in animal toxins acting on ion channels. *Biochem. J.* **378**, 717–726
- Tytgat, J., Chandy, K. G., Garcia, M. L., Gutman, G. A., Martin-Eauclaire, M. F., van der Walt, J. J., and Possani, L. D. (1999) A unified nomenclature for short-chain peptides isolated from scorpion venoms: Alpha-KTx molecular subfamilies. *Trends. Pharmacol. Sci.* **20**, 444–447
- Fajloun, Z., Mosbah, A., Carlier, E., Mansuelle, P., Sandoz, G., Fathallah, M., di Luccio, E., Devaux, C., Rochat, H., Darbon, H., De Waard, M., and Sabatier, J. M. (2000) Maurotoxin versus P11/HsTx1 scorpion toxins. Toward new insights in the understanding of their distinct disulfide bridge patterns. *J. Biol. Chem.* **275**, 39394–39402
- Dauplais, M., Lecoq, A., Song, J., Cotton, J., Jamin, N., Gilquin, B., Roumestand, C., Vita, C., de Medeiros, C. L., Rowan, E. G., Harvey, A. L., and Menez, A. (1997) On the convergent evolution of animal toxins. Conservation of a diad of functional residues in potassium channel-blocking toxins with unrelated structures. *J. Biol. Chem.* **272**, 4302–4309
- Lambert, P., Kuroda, H., Chino, N., Watanabe, T. X., Kimura, T., and Sakakibara, S. (1990) Solution synthesis of charybdotoxin (ChTX), a K⁺-channel blocker. *Biochem. Biophys. Res. Commun.* **170**, 684–690
- Stehling, E. G., Sforca, M. L., Zanchin, N. I., Oyama, S. J., Pignatelli, A., Belluzzi, O., Polverini, E., Corsini, R., Spisni, A., and Pertinhez, T. A. (2012) Looking over toxin-K(+) channel interactions. Clues from the structural and functional characterization of alpha-KTx toxin Tc32, a Kv1.3 channel blocker. *Biochemistry* **51**, 1885–1894
- Mouhat, S., Mosbah, A., Visan, V., Wulff, H., Delepierre, M., Darbon, H., Grissmer, S., De Waard, M., and Sabatier, J. M. (2004) The 'functional' dyad of scorpion toxin P11 is not itself a prerequisite for toxin binding to the voltage-gated Kv1.2 potassium channels. *Biochem. J.* **377**, 25–36
- Chen, P., and Kuyucak, S. (2009) Mechanism and energetics of charybdotoxin unbinding from a potassium channel from molecular dynamics simulations. *Biophys. J.* **96**, 2577–2588
- Jouirou, B., Mosbah, A., Visan, V., Grissmer, S., M'Barek, S., Fajloun, Z., Rietschoten, J. V., Devaux, C., Rochat, H., Lippens, G., El, M., De, A., Waard, M., Mabrouk, K., and Sabatier, J. M. (2004) Cobatoxin 1 from *Centruroides noxius* scorpion venom: chemical synthesis, three-

A new Kv1.3 inhibitor identified from *Xenopsylla cheopis*

- dimensional structure in solution, pharmacology and docking on K⁺ channels. *Biochem. J.* **377**, 37–49
27. Villalonga, N., Escalada, A., Vicente, R., Sanchez-Tillo, E., Celada, A., Solsona, C., and Felipe, A. (2007) Kv1.3/Kv1.5 heteromeric channels compromise pharmacological responses in macrophages. *Biochem. Biophys. Res. Commun.* **352**, 913–918
 28. Vicente, R., Villalonga, N., Calvo, M., Escalada, A., Solsona, C., Soler, C., Tamkun, M. M., and Felipe, A. (2008) Kv1.5 association modifies Kv1.3 traffic and membrane localization. *J. Biol. Chem.* **283**, 8756–8764
 29. Leanza, L., Henry, B., Sassi, N., Zoratti, M., Chandy, K. G., Gulbins, E., and Szabo, I. (2012) Inhibitors of mitochondrial Kv1.3 channels induce Bax/Bak-independent death of cancer cells. *EMBO Mol. Med.* **4**, 577–593
 30. Gulbins, E., Sassi, N., Grassme, H., Zoratti, M., and Szabo, I. (2010) Role of Kv1.3 mitochondrial potassium channel in apoptotic signaling in lymphocytes. *Biochim. Biophys. Acta* **1797**, 1251–1259
 31. Blunck, R., Scheel, O., Muller, M., Brandenburg, K., Seitzer, U., and Seydel, U. (2001) New insights into endotoxin-induced activation of macrophages: Involvement of a K⁺ channel in transmembrane signaling. *J. Immunol.* **166**, 1009–1015
 32. Li, W., Huang, H., Zhang, Y., Fan, T., Liu, X., Xing, W., and Niu, X. (2013) Anti-inflammatory effect of tetrahydrocoptisine from *Corydalis impatiens* is a function of possible inhibition of TNF- α , IL-6 and NO production in lipopolysaccharide-stimulated peritoneal macrophages through inhibiting NF- κ B activation and MAPK pathway. *Eur. J. Pharmacol.* **715**, 62–71
 33. Vinegar, R., Schreiber, W., and Hugo, R. (1969) Biphasic development of carrageenin edema in rats. *J. Pharmacol. Exp. Ther.* **166**, 96–103
 34. Loram, L. C., Fuller, A., Fick, L. G., Cartmell, T., Poole, S., and Mitchell, D. (2007) Cytokine profiles during carrageenan-induced inflammatory hyperalgesia in rat muscle and hind paw. *J. Pain* **8**, 127–136
 35. Nguyen, T., Chen, X., Chai, J., Li, R., Han, X., Chen, X., Liu, S., Chen, M., and Xu, X. (2020) Antipyretic, anti-inflammatory and analgesic activities of *Periplaneta americana* extract and underlying mechanisms. *Biomed. Pharmacother.* **123**, 109753
 36. Roome, T., Dar, A., Naqvi, S., Ali, S., and Choudhary, M. I. (2008) *Aegiceras corniculatum* extract suppresses initial and late phases of inflammation in rat paw and attenuates the production of eicosanoids in rat neutrophils and human platelets. *J. Ethnopharmacol.* **120**, 248–254
 37. Matzner, N., Zemtsova, I. M., Nguyen, T. X., Duszenko, M., Shumilina, E., and Lang, F. (2008) Ion channels modulating mouse dendritic cell functions. *J. Immunol.* **181**, 6803–6809
 38. Wu, B. M., Liu, J. D., Li, Y. H., and Li, J. (2020) Margatoxin mitigates CCl₄-induced hepatic fibrosis in mice via macrophage polarization, cytokine secretion and STAT signaling. *Int. J. Mol. Med.* **45**, 103–114
 39. Emanuelsson, O., Brunak, S., von Heijne, G., and Nielsen, H. (2007) Locating proteins in the cell using TargetP, SignalP and related tools. *Nat. Protoc.* **2**, 953–971
 40. Kim, D. E., Chivian, D., and Baker, D. (2004) Protein structure prediction and analysis using the Robetta server. *Nucleic Acids Res.* **32**, W526–W531
 41. Schwede, T., Kopp, J., Guex, N., and Peitsch, M. C. (2003) SWISS-MODEL: An automated protein homology-modeling server. *Nucleic Acids Res.* **31**, 3381–3385
 42. Chen, R., Li, L., and Weng, Z. (2003) ZDOCK: An initial-stage protein-docking algorithm. *Proteins* **52**, 80–87
 43. Zhang, B., Deng, Z., Zeng, B., Yang, S., Chen, X., Xu, X., and Wu, J. (2018) In-vitro effects of the FS50 protein from salivary glands of *Xenopsylla cheopis* on voltage-gated sodium channel activity and motility of MDA-MB-231 human breast cancer cells. *Anticancer. Drugs* **29**, 880–889
 44. Zeng, B., Chai, J., Deng, Z., Ye, T., Chen, W., Li, D., Chen, X., Chen, M., and Xu, X. (2018) Functional characterization of a novel lipopolysaccharide-binding antimicrobial and anti-inflammatory peptide *in vitro* and *in vivo*. *J. Med. Chem.* **61**, 10709–10723
 45. Deng, Z., Chai, J., Zeng, Q., Zhang, B., Ye, T., Chen, X., and Xu, X. (2019) The anticancer properties and mechanism of action of tablysin-15, the RGD-containing disintegrin, in breast cancer cells. *Int. J. Biol. Macromol.* **129**, 1155–1167
 46. Livak, K. J., and Schmittgen, T. D. (2001) Analysis of relative gene expression data using real-time quantitative PCR and the 2⁻($\Delta\Delta$ C_T) Method. *Methods* **25**, 402–408